International Journal of Concrete Structures and Materials

RESEARCH Open Access

Maximum Shear Strength Limit for Reinforced Concrete Deep Beams

Jung-Yoon Lee[1], Yeonje Choi[2] and Donglk Shin[3*]

Abstract

Although it is widely known that the shear strength of reinforced concrete (RC) deep beams is higher than that of general RC beams to which Bernoulli's assumption can be applied, the maximum shear strength limit of deep beams is identical to that of general beams. Therefore, the shear strength of deep beams is limited to a low value due to the shear strength limit in many cases. Different codes currently in use have different limit values for the maximum shear strength of deep beams. The strength limit of deep beams in the ACI 318–19 code is a function of the square root of concrete compressive strength ($\sqrt{f_c'}$), but that in the AASHTO-LRFD code is a linear function of f_c'. Therefore, the ACI 318–19 code tends to underestimate the shear strength of deep beams with high-strength concrete. In addition, because the strength limits of the two codes do not consider the influences of the shear span-to-depth ratio, they may overestimate the strength of large-size deep beams with a large shear span-to-depth ratio. In this study, an equation for evaluating the maximum shear strength limit of deep beams was developed and verified against the experimental results, considering the effective compressive strength of concrete, shear span-to-depth ratio. The proposed maximum strength limit of deep beams was compared with the shear strengths of 672 deep beams, and the results indicated that the prediction closely matched the measured strength limit. The coefficient of variation of the shear strength ratio of ACI318-19 code was 39.2%, while that of the proposed equation was 32.3%, which was the smallest among the three predictions.

Keywords Deep beams, Shear span-to-depth ratio, High strength concrete, Maximum shear strength, Compressive strength of concrete

1 Introduction

In the ACI 318–99 code (1999), the design of deep beams is based on the research results of Paiva and Siess (1965) and Crist (1966). This method was changed to design based on the Strut-and-Tie Model (STM) or design that considers the nonlinear strain distribution in the ACI 318–02 code (2002). The STM provides design engineers with a flexible and intuitive option for designing deep beams (Brown, 2005). The STM is widely applied in the design of bridges, deep beams, corbels, end tabs, and walls with openings et al. (ACI Committee 445, 2002; Foster & Gilbert, 1998). The STM is used in the ACI 318–19 code (2019) as well as the EC2-04 (2004), CSA-19 (2019), and AASHTO-LRFD codes (2020). The basic concept of STM used in the four codes is almost similar, but different regulations are applied for the maximum strength limit of deep beams. The maximum shear strength ($V_{n,max}$) of the general beams (shear span-to-depth ratio, $a/h \geq 2.0$) in the ACI318-19 code (2019) is

Journal information: ISSN 1976-0485 / eISSN 2234-1315.

*Correspondence:
Donglk Shin
s91120@naver.com
[1] School of Civil, Architectural Engineering and Landscape Architecture at Sungkyunkwan University, 2066, Seobu-Ro, Jangan-Gu, Suwon-Si, Gyeonggi-Do 16419, Republic of Korea
[2] Department of Civil, Architectural, and Environmental System Engineering at Sungkyunkwan University, 2066, Seobu-Ro, Jangan-Gu, Suwon-Si, Gyeonggi-Do 16419, Republic of Korea
[3] Global Engineering Institute for Ultimate Society at Sungkyunkwan University, 2066, Seobu-Ro, Jangan-Gu, Suwon-Si, Gyeonggi-Do 16419, Republic of Korea

proportional to $\sqrt{f_c'}$, while that of EC2-04 (2004), CSA-19 (2019), and AASHTO-LRFD codes (2020) is proportional to f_c'. The ACI318-19 code (2019) employs an empirically derived relationship to limit the maximum shear strength, while the other codes use equations based on the force equilibrium between the diagonal concrete strut and the shear reinforcement of the truss model. For the $V_{n,max}$ of the deep beams ($a/h < 2.0$), empirical limits are used in the ACI 318–19 (2019) and AASHTO-LRFD codes (2020), whereas the EC2-04 (2004) and CSA-19 codes (2019) do not specify a maximum shear strength limit of deep beams. Consequently, there is a difference between the two types of limits for the maximum shear strength ($V_{n,max}$) of deep beams. In the ACI 318–19 code (2019), $V_{n,max}$ is proportional to $\sqrt{f_c'}$, but in the AASHTO-LRFD code (2020), it increases in proportion to f_c'. Therefore, both $V_{n,max}$ are similar for members with normal-strength concrete but significantly different for members with high-strength concrete. In particular, despite the increase in deep beams that use high-strength concrete (e.g., Foster and Gilbert (1998) and Shin et al. (1999)) and fiber reinforced concrete deep beams with high tensile strength (Sandeep et al.2022; Bediwy & El-Salakawy, 2021), the $V_{n,max}$ of the ACI 318–19 code (2019) cannot accurately predict the maximum strength of such members. Consequently, the strength of such deep beams is limited by the $V_{n,max}$ in many cases, resulting in a conservative design. In addition, the strength of deep beams increases as the shear span-to-depth ratio (a/h) decreases, but the limits of the ACI 318–19 (2019) and AASHTO-LRFD codes (2020) are constant regardless of a/h. Therefore, they conservatively limit the strength of deep beams with small a/h values. Conversely, the two codes excessively limit the strength of deep beams with large a/h values.

In the ACI 318–19 code (2019), the shear strength limit of RC deep beams that belong to the D-region ($V_{n,max} \le 5/6\sqrt{f_c'}b_w d$) is identical to that of general beams that belong to the B-region. The regulation of $V_{s,max} \le 2/3\sqrt{f_c'}b_w d$ is used for general beams. If the shear strength provided by concrete ($V_c \le 1/6\sqrt{f_c'}b_w d$) is added to this, the maximum shear strength of general beams becomes identical to that of deep beams ($V_{n,max} \le 5/6\sqrt{f_c'}b_w d$). The concrete shear resistance of deep beams generally greater than that of general beams (Kong, 1990; Tan & Cheng, 2006). Nevertheless, the $V_{n,max}$ of deep beams is regulated in the same manner as that of general beams. This indicates that the $V_{n,max}$ of deep beams can be limited conservatively.

Many studies have been conducted thus far, on the shear strength of deep beams. In most of them, the influence of the shear span-to-depth ratio (Larson et al., 2013; Smith & Vantsiotis, 1982), concrete compressive strength (Foster & Gilbert, 1998; Yang et al., 2003), presence/absence of shear reinforcement (Russo et al., 2005), presence/absence of horizontal reinforcement (Rogowsky et al., 1986), and size-effect (Tan & Cheng, 2006; Zhang & Tan, 2007) on the shear behavior was evaluated. Moreover, some studies have been conducted on the shear strength of recycled aggregate concrete beams and shear crack-induced deformation (Imjai et al., 2016, 2023, 2024). However, there have been limited studies on the maximum strength limit of deep beams. Proestos et al. (2018) indicated that the maximum shear strength limits of the ACI 318–19 code (2019) significantly underestimated the shear strength of high strength concrete members with large quantities of shear reinforcement or short shear spans. Hwang et al. (2021) proposed a softened STM for determining the maximum shear strength of deep beams. Their results indicated that the ACI 318–19 (2019) limit appeared to be short of the design parameters of the strut inclination angle and the amount of longitudinal tensile reinforcement. However, these studies did not specifically present the influencing factors and an evaluation method of the maximum strength limit of deep beams.

Lee and Hwang (2010) examined $V_{s,max} \le 2/3\sqrt{f_c'}b_w d$ for general beams specified in the ACI 318–19 code (2019). According to the experimental results, $V_{s,max}$ was affected by the compressive strength of concrete and the amount of shear reinforcement, and the $V_{s,max}$ of the ACI 318–19 code (2019) was conservative compared with those of the EC2-04 (2004) and CSA-19 codes (2019). This study presented a method for evaluating the $V_{s,max}$ of general beams with a shear span-to-depth ratio of 2 or more, but did not address a method for evaluating the maximum strength limit of deep beams.

To reasonably predict $V_{n,max}$ of deep beams, the effects of the influencing factors on the shear strength should be included in the $V_{n,max}$ evaluation equation. The results of previous studies indicated that the maximum shear strength limit in the ACI 318–19 code (2019) did not clearly reflect the shear strength of deep beams. In this study, factors affecting the maximum shear strength of deep beams were identified by analyzing a large experimental data of 672 specimens, reported in the previous literature. Based on the analysis, a theoretical model for calculating the maximum shear strength of deep beams was proposed and verified against the experimental data. The proposed model considered the effect of compressive strength of concrete and shear span-to-depth ratio on the maximum shear strength of deep beams. The proposed equation may allow a safe and economical design of deep beams compared to the existing models for maximum shear strength limit.

2 Analysis of Maximum Shear Strength of Deep Beams

Fig. 1a presents the maximum shear strength limits specified in the ACI 318–19 (2019) and AASHTO-LRFD codes (2020) for deep beams. As mentioned in the previous section, the $V_{n,max}$ of the ACI 318–19 code (2019) is proportional to $\sqrt{f_c'}$, but that of the AASHTO-LRFD code (2020) ($V_{n,max} = 0.225 b_w d f_c'$) is proportional to f_c'. Fig. shows that the difference in $V_{n,max}$ between the two codes at $f_c' = 20$ MPa is approximately 1.21 times, but it increases to 2.09 times at $f_c' = 60$ MPa. Since the EC2-04 (2004) and CSA-19 codes (2019) do not include provisions for $V_{n,max}$ of deep beams, this study compares shear strength of the concrete strut ($V_{n,strut}$) in the STM, as shown in Fig. 1b. In the Fig., for a fixed value of f_c' at 40 MPa, the $V_{n,strut}$ of the EC2-04 (2004) and CSA-19 codes (2019) is higher than the $V_{n,max}$ of the ACI 318–19 code (2019) when a/h is small, but the opposite is true when a/h is large. This is because the limit of the ACI 318–19 code (2019) is constant regardless of a/h, but the vertical component of the concrete strut strength changes according to the angle of the strut.

Previous studies (Hwang et al., 2021; Proestos et al., 2018) revealed various influence factors i.e. concrete strength, shear-span-to-depth ratio, size effect etc. which affect the maximum shear strength of deep beams. None of the current design codes account for the effect of these factors in their formulation for maximum shear strength limit. Considering the inconsistent approaches adopted in the codes, a detailed analysis was carried out in this study to evaluate the factors that affect $V_{n,max}$ using experimental data of 672 deep beams, accumulated from the existing literature. The data included 362 specimens with vertical shear reinforcement, and 176 specimens with horizontal reinforcement. The a/h was distributed between 0.25 and 2.0, as shown in Fig. 2. A total of 71 specimens had $a/h \leq 0.5$, 475 specimens had $0.5 < a/h \leq 1.5$, and 126 specimens had $1.5 < a/h \leq 2.0$. The concrete compressive strength (f_c') mainly ranged from 20 to 40 MPa, but in 51 specimens, high-strength concrete with f_c' greater than 60 MPa was used. To evaluate the influence of the size-effect, 79 specimens with a section depth (h) greater than 1000 mm were analyzed. The longitudinal (ρ_w), vertical (ρ_v), and horizontal shear reinforcement ratios (ρ_h) are shown in Fig. 2. Table 1 presents the description of the test results, and details of the specimens can be found elsewhere (Lee & Kang, 2021). In addition, the reference details of the original sources of the test results are present in the Appendix.

2.1 Influence of Concrete Compressive Strength

It is widely known that the strength of deep beams is affected by a/h, f_c', and h (Kong, 1990; Tan & Cheng, 2006). In this study, 85 specimens with similar properties except f_c' were selected from the 672 specimens, and the experimental results were analyzed to evaluate the influence of the compressive strength of concrete on $V_{n,max}$. For the 85 specimens, h was approximately 500 mm and a/h was approximately 0.9, but f_c' varied to 60 MPa. The longitudinal tensile reinforcement ratio ranged from 0.0033 to 0.0383 and the vertical shear reinforcement ratio ranged from 0 to 0.0132.

Fig. 3a and b show the results for the shear strength ($v_{test} = V_{test}/(bd)$) of 85 specimens nondimensionalized by f_c' and $\sqrt{f_c'}$, respectively. The lines in the figures represent the regression fitting lines. When the shear strength

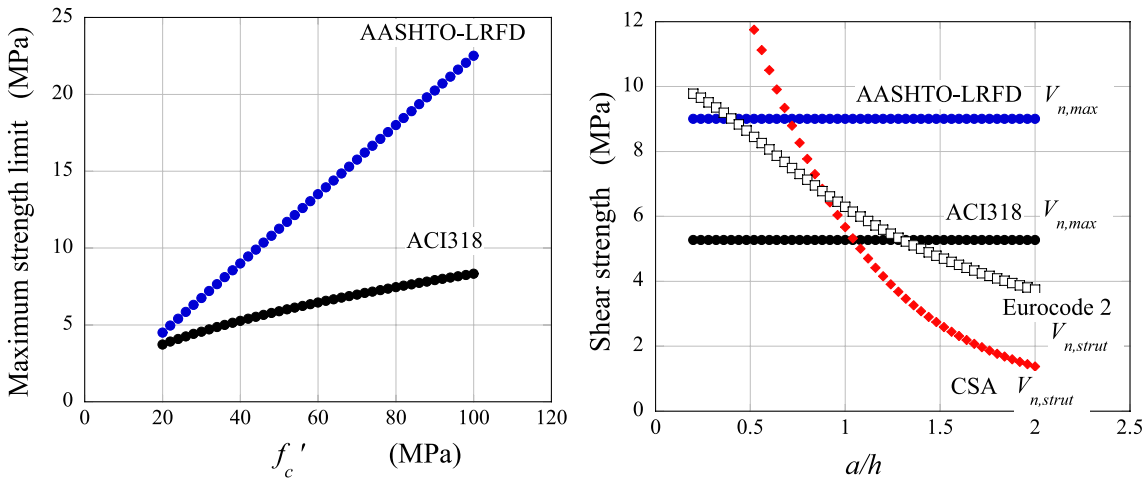

Fig. 1 Comparison of the maximum shear strength limits of deep beams

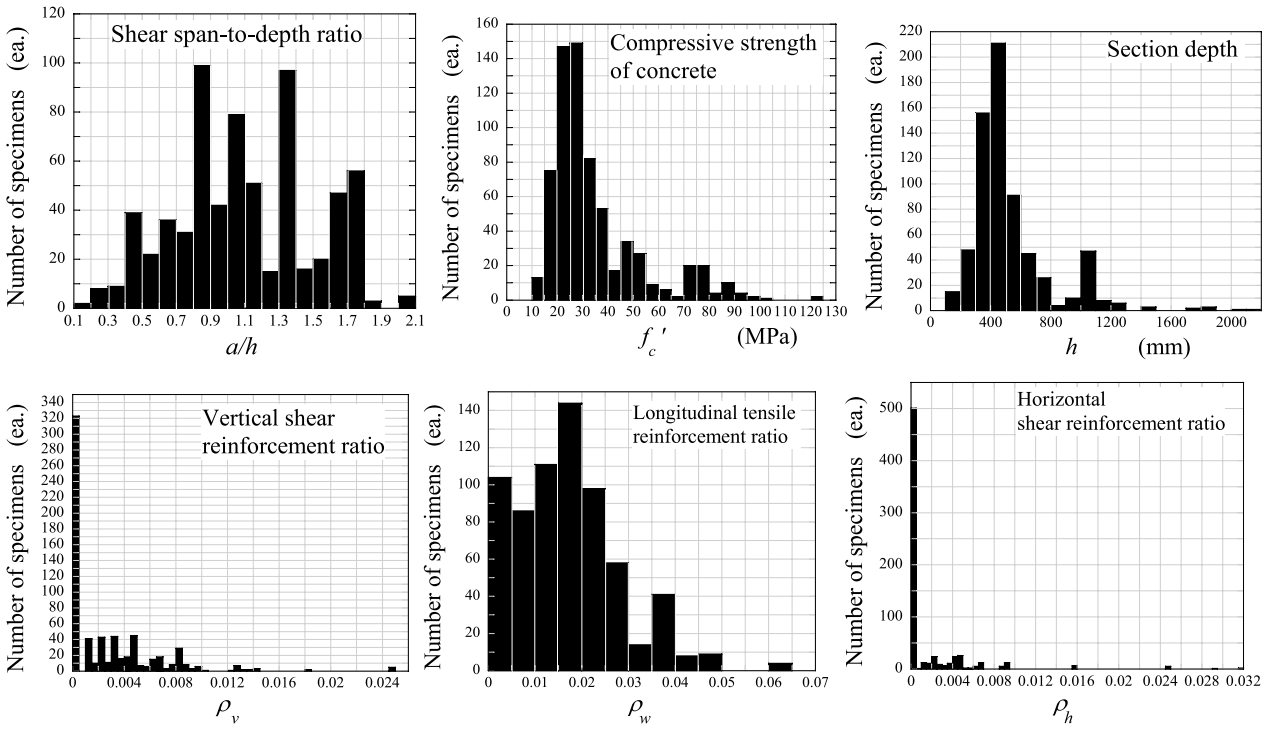

Fig. 2 Variable distributions of the 672 specimens

was nondimensionalized by f_c', v_{test} remained almost constant with an increase in f_c', as shown in Fig. 3a. However, when the shear strength was nondimensionalized by $\sqrt{f_c'}$, $v_{test}/\sqrt{f_c'}$ increased with $\sqrt{f_c'}$, as shown in Fig. 3b, indicating that it was still affected by the concrete strength.

As shown in Fig. 4, the shear strengths of the specimens and $v_{n,max}$ of the two codes were compared to evaluate the influence of f_c' on $v_{n,max}$. Given that the failure mode of the specimen can influence v_{test}, 85 specimens in Fig. 4 were classified according to their failure mode. Among them, 3 specimens failed due to flexural yielding, while the others failed due to web concrete crushing. When predicting v_{test}, it may be desirable for the predicted strength to be lower than the actual strength for design safety. However, since $v_{n,max}$ is the maximum limit of v_{test}, $v_{n,max}$ should be positioned at the upper limit of v_{test}, rather than at the average value of v_{test} (Proestos et al., 2018). As shown in Fig. 4, the $v_{n,max}$ of the ACI 318–19 code (2019) was lower than v_{test} in many cases regardless of the failure mode. In particular, when f_c'≥35 MPa, $v_{n,max}$ was lower than v_{test} in most cases. This indicates that the $v_{n,max}$ of the ACI 318–19 code (2019) is conservative. In contrast, the $v_{n,max}$ of the AASHTO-LRFD code (2020) was higher than v_{test} in most cases, indicating that the maximum values of the specimens were accurately predicted. Among the 85 specimens analyzed, the maximum shear strength, $v_{n,max}$ predicted by the ACI 318–19 code was lower than the experimental shear strength, v_{test} in 65 cases (76.5%), whereas the AASHTO-LRFD code underestimated v_{test} in only 12 cases (14.1%). As f_c' increased, the $v_{n,max}$ of the AASHTO-LRFD code (2020) maintained a constant difference from v_{test}, but the difference between the $v_{n,max}$ of the ACI 318–19 code (2019) and v_{test} increased. For example, when f_c'=20MPa and 50MPa, the $v_{test}/v_{n,max}$ of the ACI 318–19 code were 0.82 and 1.35, respectively, while those of AASHTO-LRFD code were 0.67 and 0.71, respectively.

2.2 Influence of Shear Span-to-Depth Ratio

In this study, 34 specimens with similar properties except a/h were selected from the 672 specimens, and the experimental results were analyzed to evaluate the influence a/h on $v_{n,max}$. For the 34 specimens, the section depth (h) varied from 250 to 600 mm, f_c' from 40 to 55MPa, and a/h from 0.25 to 2. The longitudinal tensile reinforcement ratio ranged from 0.0123 to 0.0476 and the vertical shear reinforcement ratio ranged from 0 to 0.0181.

For the ACI 318–19 (2019) and AASHTO-LRFD codes (2020), $v_{n,max}$ was constant regardless of a/h, but the strength of deep beams decreased as a/h increased (Brown, 2005). Fig. 5 shows the relationship between the experimental strength (v_{test}) and a/h for the 34 specimens. Given that the failure mode of the specimen can

Table 1 Material properties of the 672 specimens

Reference	Description
Rogowsky et al (1986)	The test specimens consisted of RC beams with varying cross-sections, encompassing both simple span and two-span configurations
Clark (1951)	The principal variables included the ratio of beam depth to shear span, the ratio of web reinforcement, the quantity of tensile reinforcement, and the concrete strength
Moody et al (1954)	Simple rectangular beams were tested. These beams featured three distinct tension reinforcement percentages. Among the subset of beams lacking web reinforcement, half were fabricated with hooks
Moody et al (1955)	All beams were reinforced with an intermediate-grade deformed bar with equal quantities of longitudinal steel both at the bottom and the top
Morrow and Viest (1957)	All beams had a reinforced column stub cast integrally at midspan, and one or two external stirrups placed at each end outside the span to prevent failure by splitting at the level of reinforcement
Chang and Kesler (1958)	The specimen was an RC beam with relatively compact cross-sections measuring 4 × 6 inches, featuring only tensile reinforcement. The study examined the static and fatigue strength of the beam across various loading conditions
Watstein and Mathey (1958)	RC beams that designed to fail in shear had a cross-section of 8 × 18 in., a 6-ft span, and were loaded at third points
Rodriguez et al (1959)	The specimens consisted of two-span continuous RC beams, featuring a rectangular cross-section measuring 8 in. × 16 in. and extending to a length of 12 ft. The experiment was designed to assess the shear strength of these beams across various loading conditions
De Cossio and Siess (1960)	Two RC deep beams exhibited a cross-section measuring 8 × 18 inches. The height-to-shear span ratio (a/h) for these beams was 1.38 and 1.67, respectively
Mathey and Watstein (1963)	RC beams lacking web reinforcement were cast within steel forms, placing the tensile reinforcement near the bottom. The key variables encompassed six types of deformed bars, each with varying yield strengths
Kani (1967)	Experiments were performed using various cross-sectional dimensions and a/d ratios as variables
Ramakrishnan and Ananthanarayana (1968)	A single-span rectangular deep beam with a height-to-span ratio of more than 1/2 was tested under different loading conditions, such as two-point loading, uniformly distributed loading, and centrally concentrated loading
Smith and Vantsiotis (1982)	All specimens were reinforced with high-strength deformed bars and had a cross-section measuring 4 × 14 inches. The experiments were conducted with various a/d ratios
Mphonde and Frantz (1984)	The cross-section of the slender beams remained consistent at 6 × 13.25 inches; however, there was a variation in concrete strength, with values of 23.1 and 79.5 MPa
Kong et al (1970)	The specimens had a constant width of 3 inches and heights of 10, 15, 20, 25, and 30 inches. The main variables were the number of vertical stirrups and horizontal stirrups
Foster and Gilbert (1998)	Eleven RC deep beams, constructed using high-strength concrete with a maximum aggregate size of 10 mm, underwent testing. The majority of the specimens featured a cross-section of 124.5 × 701 mm, with a/d ratios ranging from 0.5 to 1.32
Alcocer and Uribe (2008)	RC beams were designed to measure the monolithic and cyclic behavior of deep beams. A major feature of the beams was that the ends are covered with a polyurethane sheathing sealed with silicone and placed 320 mm (13 in.) above the end of the main longitudinal bars
Walravena and Lehwalter (1994)	The beam depth was varied between 200 and 1000 mm and all other variables were kept constant. The specimens were designed to avoid failure due to longitudinal steel yield
Xie et al (1994)	The RC beam was 5 inches wide and 10 inches deep. The ratio of shear span to depth was 1 and 2. There were no reinforcements other than tensile steel
Tan et al (1995)	Fifteen RC deep beams featured a rectangular cross-section measuring 500 mm in depth and 110 mm in width. The effective span ranged from 1000 to 2500 mm
Shin et al (1999)	The specimens consisted of high-strength concrete beams with varying strengths (7600 and 10,600 psi) and a/d ratios of 1.5, 2.0, and 2.5. These beams maintained a consistent cross-sectional size (125 mm × 250 mm) and a longitudinal reinforcement ratio of 0.0377
Tan and Lu (1999)	Simply supported RC deep beams featured a cross-section with a width of 140 mm and heights ranging from 500 to 1750 mm. To avoid flexural failure, a 2.60% main steel ratio was utilized
Pendyala and Mendis (2000)	The primary variables of the beams include distinct shear span-depth ratios (2 and 5), varying stirrup spacing (70, 140, and 210 mm), and nominal concrete strength ranging from 30 to 100 MPa
Oh and Shin (2001)	Rectangular deep beams, featuring a cross-section of 130 × 560 mm and an effective depth of 500 mm, were subjected to testing to assess their diagonal cracking and ultimate shear capacities, considering a range of concrete compressive strengths from 23.7 to 73.6 MPa
Tan et al (1997)	All the beams were made of high-strength concrete (HSC) with a compressive strength greater than 55 MPa. The main variables were the ratio and the yield strength of the vertical and horizontal web reinforcement

Table 1 (continued)

Reference	Description
Paul and Rangan (1998)	Reinforced simply supported high-performance concrete beams, equipped with vertical shear reinforcement, underwent testing subjected to a concentrated load at midspan to determine their shear strength
Manuel (1974)	Deep beams with web compressive failure had a cross-section of 4 × 18 inches and an effective depth of 16 inches. The test was conducted with a/d ratio and the type of the longitudinal reinforcement
de Paiva and Siess (1965)	The major variables were the amount of tension reinforcement, the concrete strength, the amount of web reinforcement and the span-depth ratios. The beams were loaded at the third points
Yang et al (2003)	21 beams had different overall depths, concrete strengths, shear span, total length, effective depth, longitudinal bars, and a/h, a/d, and l/h ratios
Zhang and Tan (2007)	The overall height of the beams was systematically varied, ranging from 350 to 1000 mm, to investigate the size-effect in RC deep beams
Matsuo et al (2002)	The cross section of the two deep beams was 149.9 × 650.2 mm, the effective depth was 599.4 mm, and a/d was constant at 1. The difference was that the vertical shear reinforcement ratios were 0.0042 and 0.0084
Lertsrisakulrat et al (2001)	The cross-section width (150 mm) and a/d ratio (1) remained consistent across three deep beams without vertical and horizontal shear reinforcement
Lehwalter (1988)	The beams exhibited longitudinal reinforcement ratios ranging from 0.0066 to 0.0169, with variations in the a/d ratio at 0.5, 1.0, and 1.5. The section widths for all the beams were kept constant at 250 mm
Ismail (2016)	The primary variables included different a/h ratios (0.75, 1.06, 1.38, 1.44) and a range of concrete compressive strengths (30.50 ~ 85.20 MPa)
Deschenes et al (2009)	Large RC deep beams were configured to replicate the bent caps of a bridge and were subjected to different conditions to induce ASR/DEF deterioration
Larson et al (2013)	Two deep beams had a rectangular cross section of 152.4 × 762 mm and the other one had a square cross section of 457.2 × 457.2 mm. The two rectangular deep beams were the same except that the lengths of the shear spans were different, and a/h was 1 and 1.5, respectively
Brown (2005)	Except for 2 beams, all 33 deep beams shared identical cross-section dimensions (299.72 × 449.6 mm) and main longitudinal reinforcement ratios (0.0033). The study incorporated variables encompassing different a/d ratios (0.5, 0.75, 1, 1.5) and concrete compressive strengths ranging from 23.2 to 97.5 MPa
Tanimura and Sato (2005)	Rectangular beams which all the same cross-sectional dimensions (190 × 320 mm) were tested to investigate the influence of the moment-shear ratio
Leonhardt and Walther (1961)	Seven deep beams lacking shear reinforcement were tested. The section width remained constant at 100 mm, while the heights varied at 300 and 600 mm. Additionally, the a/h ratios varied, specifically at 0.25, 0.33, 0.5, and 0.67
Niwa (1981)	All beams were loaded symmetrically by a single point load at mid-span, and a shear failure occurred prior to yielding of the longitudinal reinforcement. Main variables were the longitudinal reinforcement ratio and the shear span-to-effective depth ratio
Adebar (2000)	3 deep beams had the same member size, such as cross section width, height, effective depth, and shear span. The differences were concrete compressive strength (38 and 51 MPa), longitudinal reinforcement yield strength (468 and 865 MPa), and longitudinal reinforcement ratio (0.0044 and 0.0072)
Seliem et al (2006)	The beams were designed based on various parameters such as section height (500 and 900 mm), a/d (0.41 ~ 1.53), and concrete compressive strength (34.9 ~ 52 MPa)
Subedi et al (1986)	For the beams to have geometrically similar cross-sectional areas, the width of the section was increased to 50, 100, and 200 mm, and the effective depth was increased to 200, 400, and 800 mm accordingly. The shear span-to-effective depth ratio was divided into 1 and 1.5
Watanabe et al (2008)	Except for 2 beams, the total of 36 deep beams featured uniform cross-sectional dimensions (300 × 450 mm) and an effective depth of 400 mm. The primary variables under investigation encompassed distinct a/d ratios (0.5, 0.75, 1, 1.5) and a varied range of concrete compressive strengths, ranging from 23.2 to 36.8 MPa
Tanimura et al (2004)	The conducted test aimed to delve into the failure mode of the deep beam. The core variables under scrutiny included the shear span-to-effective depth ratios (0.5, 1, and 1.5) and the presence or absence of vertical shear reinforcement
Maeda et al (2008)	To investigate the shear strength of RC beams with a small shear span ratio, 11 deep beams with the same width, height, and effective depth were tested. The effective depths were 1, 1.5, and 2, and the vertical shear reinforcement ratio was varied as 0, 0.0048, 0.0084, and 0.01432
Lertsrisakulrat et al (2002)	9 rectangular deep beams with a constant a/d of 1 were tested to determine the effect of shear reinforcement on the shear behavior of RC deep beams. The principal variable was the vertical shear reinforcement ratio (0, 0.0042, 0.0084)
Seki et al (2012)	The seven deep beams were divided into two types. Five had a cross section of 300 × 450 mm and an a/d of 1.25. The other two had a cross section of 500 × 1050 mm and had a/d of 1.04 and 1.62. The two types were different in the yield strength and the ratio of the reinforcements

Table 1 (continued)

Reference	Description
Kosa et al (2009)	Deep beams without shear reinforcement were tested. The width of the section was constant at 100 mm, but the heights were 300 and 600 mm, and the a/h was varied at 0.25, 0.33, 0.5, and 0.67
Kobayashi et al (2005)	Six large RC deep beams had different member sizes and physical properties except for the a/d value of 1.5 and the longitudinal reinforcement ratio of 0.02. These beams were tested to determine the shear strength of large deep beams
Total: 672	

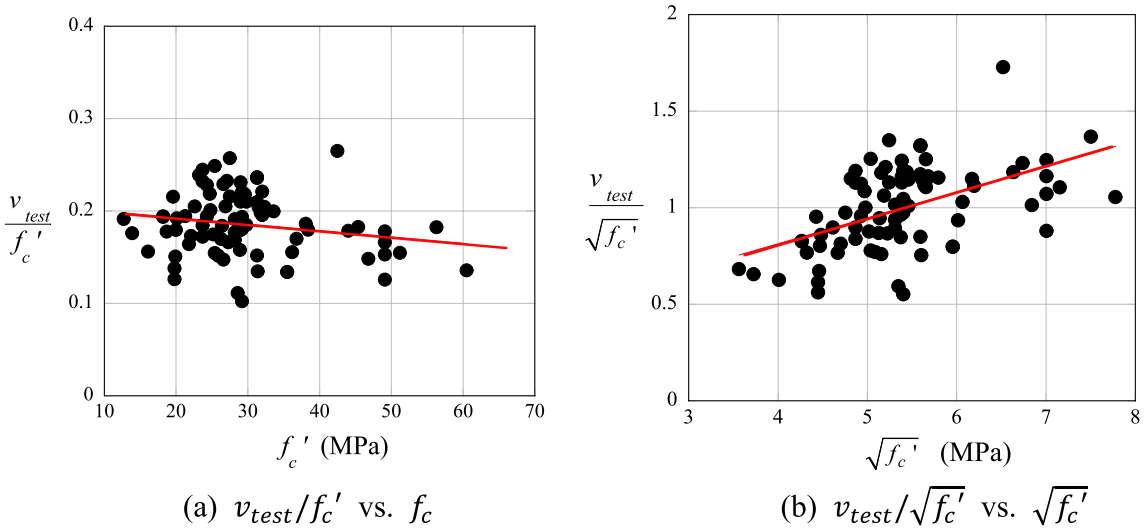

(a) v_{test}/f_c' vs. f_c (b) $v_{test}/\sqrt{f_c'}$ vs. $\sqrt{f_c'}$

Fig. 3 Effect of the concrete compressive strength on the strength of deep beams

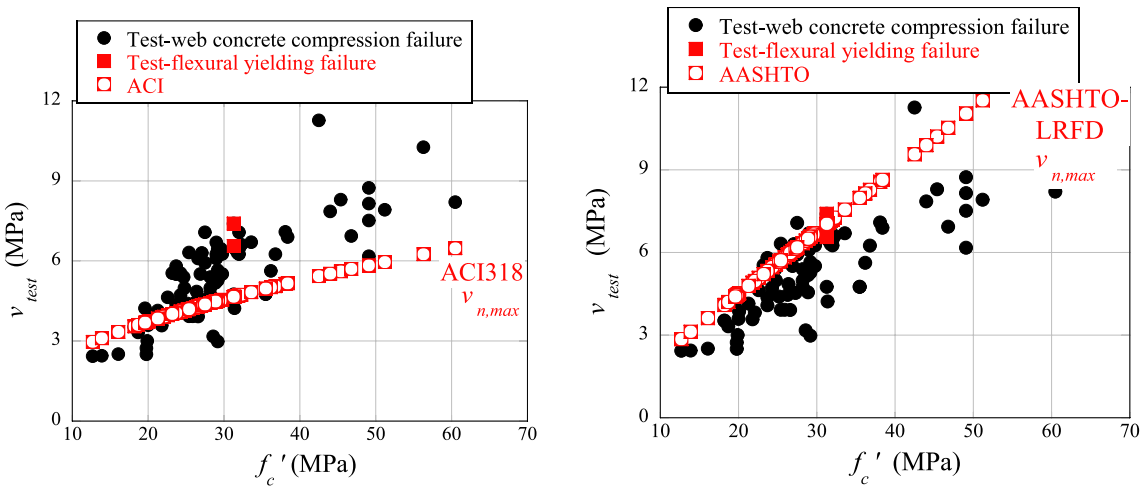

(a) ACI 318-19 code (b) AASHTO-LRFD code

Fig. 4 Relationship between $v_{n,max}$ and v_{test} for the two codes

influence v_{test}, 34 specimens in Fig. 5 were classified according to their failure mode. Among them, 11 specimens failed due to flexural yielding, while the others failed due to web concrete crushing. As shown in Fig. 5, v_{test} decreased with a constant slope as a/h increased regardless of the failure mode. Therefore, $v_{n,max}$ must also

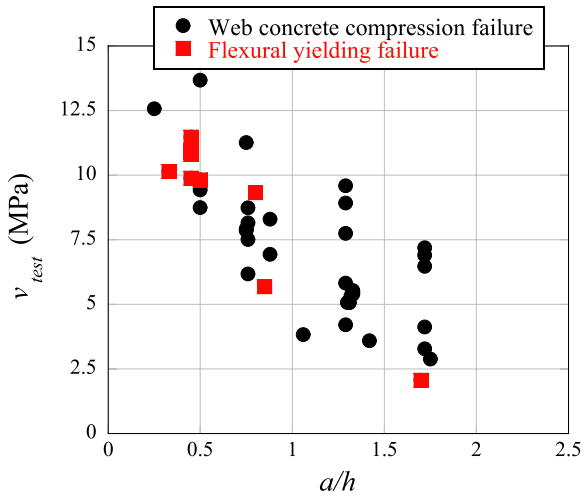

Fig. 5 Influence of a/h on v_{test}

decrease as a/h increases. Investigating the relationship between v_{test} and a/h of the 672 specimens without limiting the range of f_c', the same results as in Fig. 5 were obtained.

Fig. 6 compares v_{test} with the $v_{n,max}$ of each code. For the ACI 318–19 (2019) and AASHTO-LRFD codes (2020), $v_{n,max}$ was constant regardless of a/h. Consequently, the ACI 318–19 code (2019) evaluated the $v_{n,max}$ of the specimens with low a/h values conservatively. In contrast, the AASHTO-LRFD code (2020) overestimated the $v_{n,max}$ of the specimens with high a/h values.

2.3 Influence of Section Depth

Several previous studies (Foster & Gilbert, 1998; Smith & Vantsiotis, 1982) indicated that the section depth (h) affects the shear strength of deep beams. In the present study, the influence of h on the strength of deep beams was evaluated using the collected data. Among the 672 specimens, 143 specimens with similar properties were selected and analyzed. For these 143 specimens, a/h was approximately 0.9, but h varied to 1750 mm. The longitudinal tensile reinforcement ratio ranged from 0.0006 to 0.06 and the vertical shear reinforcement ratio ranged from 0 to 0.0191.

Fig. 7a shows the influence of h on v_{test}. Here, v_{test} was nondimensionalized through division by f_c' to exclude the influence of the f_c' on the v_{test}. Twenty one of the 143 specimens failed due to flexural yielding, and the others failed due to web concrete crushing. From Fig. 7, it can be seen that v_{test} decreased as h increased. v_{test} decreased at a constant rate until h reached 1000 mm regardless of failure mode. Fig. 7b presents the results of dividing the v_{test} of the specimens by the $v_{n,max}$ of the ACI318-19 code. As shown, $v_{test}/v_{n,max}$ decreased as h increased. This is because the size effect was not considered in the $v_{n,max}$ of the code.

3 Proposed Model for Maximum Strength of Deep Beams

The analysis of the experimental data for the 672 specimens revealed that the strength of deep beams is closely related to the compressive strength of concrete, shear span-to-depth ratio, and section depth. The $v_{n,max}$ specified in the codes is the limit on the maximum strength of the members. Thus, if these three factors affect the

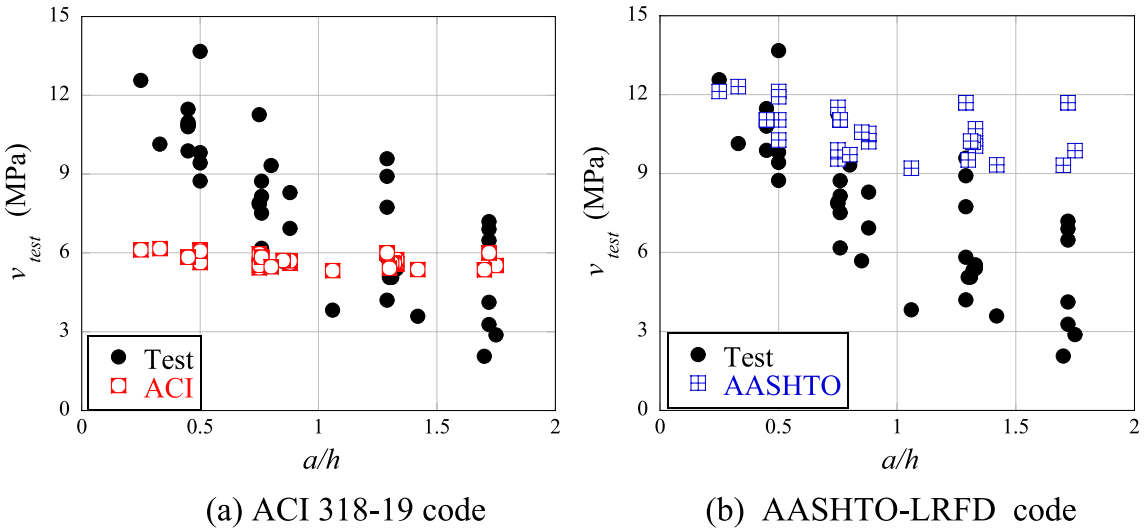

(a) ACI 318-19 code (b) AASHTO-LRFD code

Fig. 6 Relationship between a/h and v_{test}

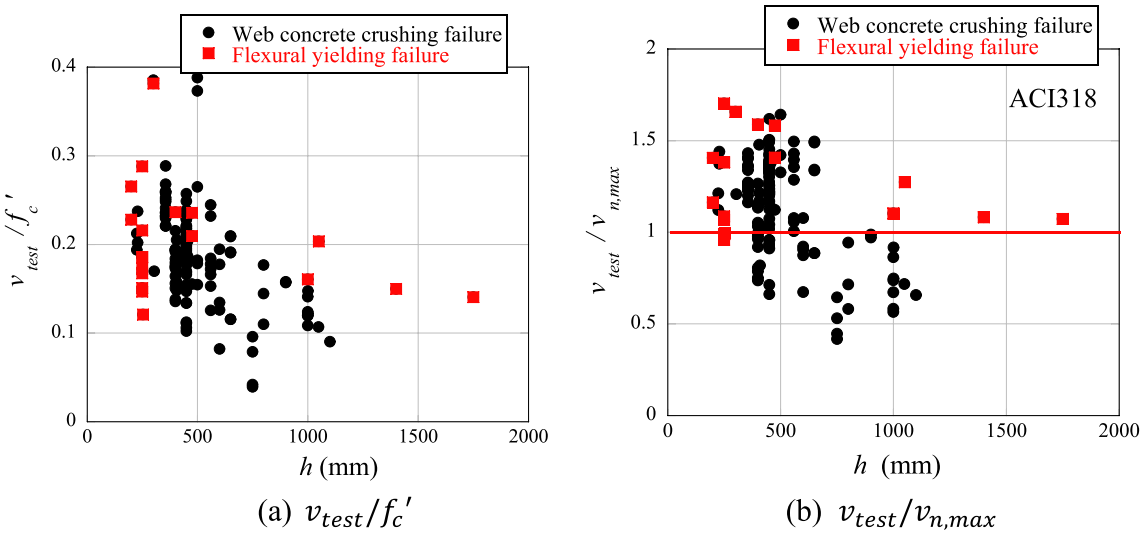

Fig. 7 Influence of h on v_{test}

strength of deep beams, it is reasonable that their effects should be included in the $v_{n,max}$ evaluation equation. In this study, the maximum strength limit evaluation equation for deep beams was developed using the Strut-Tie Model (STM).

3.1 STM for Deep Beams

To develop a maximum strength limit evaluation equation for deep beams using the STM, it is necessary to select the optimal STM for deep beams. Because the ACI 318–19 code (2019) specifies that the angle of the strut should be greater than 25° (23.2.7 in the ACI 318–19 code (2019)), the model should be selected depending on the a/h of deep beams. According to ACI Subcommittee 445 (2002), STM-1 (Fig. 8a) should be applied when a/h is small because the load transferred from the loading point to the support is large, and STM-2 (Fig. 8b) with intermediate ties should be applied when a/h is large.

According to ACI Subcommittee 445, the required amount of shear reinforcement depends on the type of STM used. Fig. 9 shows the required amount of vertical shear reinforcement ($\rho_v f_{yv}$) in each code with respect to a/h. When design was performed using STM-1 for a beam with $a/h \leq 0.5$ and STM-2 for a beam with $a/h >$ 0.5, a discontinuity occurred in the calculated required amount of shear reinforcement at point AB ($a/h = 0.5$) in the figure. This is because only the minimum vertical shear reinforcement ($\rho_{v,min} f_{yv}$) can be placed for a member with $a/h \leq 0.5$ when design is performed using STM-1, whereas vertical shear reinforcement for V_s must be placed in the deep beam when design is performed using STM-2. The discontinuity in the amount of reinforcement implies that discontinuity also occurs in the strength of the deep beam calculated via this model. Therefore, the $v_{n,max}$ of the deep beam calculated via this model may also involve discontinuity.

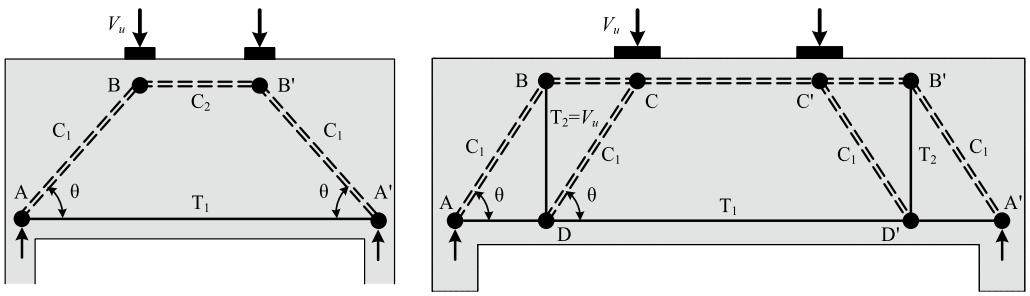

Fig. 8 Two Strut-Tie Models

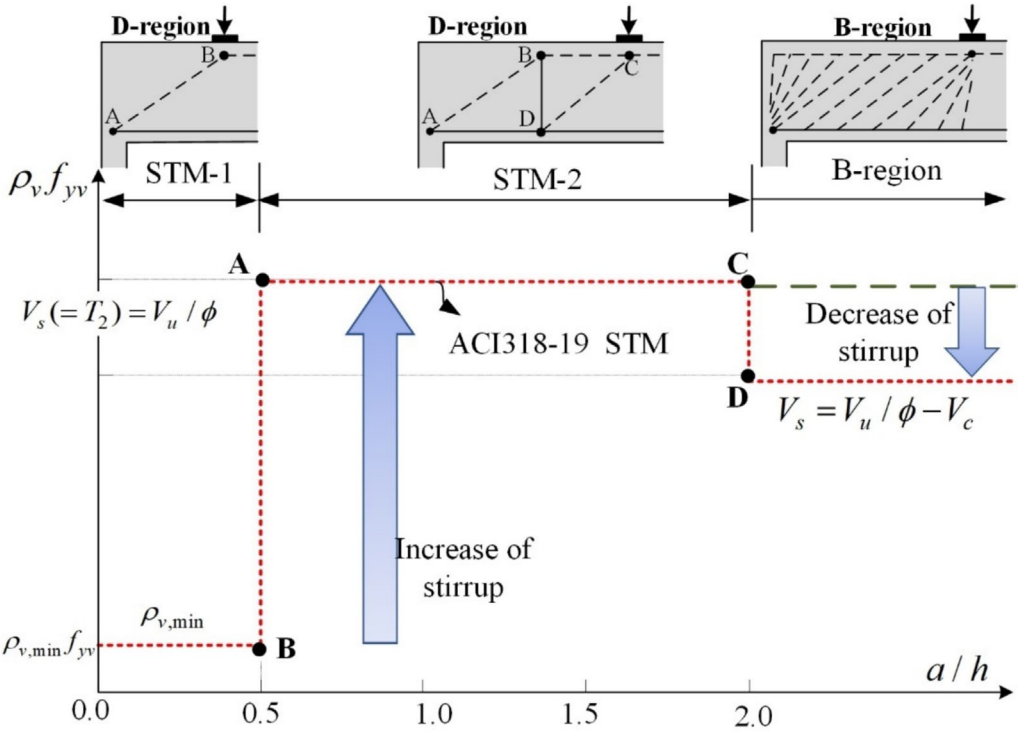

Fig. 9 Differences in the required amount of vertical reinforcement and strength depending on the model

The ACI 318–19 code (2019) divides the design of beams into the B-region and the D-region. Design using an STM is suggested for members with $a/h \leq 2$, and design using $V_n = V_c + V_s$(shear strength = shear strength of concrete + shear strength of shear reinforcement) based on the truss model is suggested when $a/h >$ 2. Members with $a/h = 2$ can be designed using the STM and the equation$V_n = V_c + V_s$, which corresponds to the B-region design method. Therefore, the results calculated via the two models of the ACI 318–19 code (2019) for members with $a/h = 2$ should be identical, but they are not. When the calculation is performed using STM-2, the member strength of vertical tie BD in Fig. 8b is identical to the factored load V_u ($V_u/\phi = T_2 = V_s$) (T_2= tensile force of vertical tie, STM design examples in the ACI 445 (2002)). When the calculation is performed using the B-region design method,$V_u = \phi(V_c + V_s)$, and the amount of vertical shear reinforcement required by the STM is always larger than that required by the B-region design method ($V_s = V_u/\phi - V_c$) (Lee & Kang, 2021). Thus, a difference in concrete shear strength (V_c) between the two calculation methods occurs, as indicated by point CD in Fig. 9. The ACI 318–19 code (2019) specifies $V_{n,max} = 5/6\sqrt{f_c'}b_w d$ as the maximum strength limit for both deep beams and general beams. However, if the strength of members with $a/h = 2$ depends on the selected method, as shown in Fig. 9, a contradiction occurs, and one of the methods is unsuitable for determining the maximum strength. In addition, when the shear force of deep beams is calculated using STM-2, all of the shear force is supported by the vertical tie ($V_u/\phi = T_2$). Thus, it is inevitable to place excessive vertical shear reinforcement (Lee & Kang, 2021).

3.2 Force Transfer by Direct Struts

The ACI 318–19 code (2019) specifies that the STM should be applied differently depending on a/h. However, a significant discontinuity occurs in the calculated amount of reinforcement and strength at the boundary between STM-1 and STM-2, as indicated by point AB in Fig. 9. To resolve such a discontinuity, it is necessary to apply the statically indeterminate STM (hereinafter referred to as STM-3) shown in Fig. 10, which is used in the CEB-FIP model code (1993) and was employed in previous studies (Foster, 1998; Foster & Gilbert, 1998). In STM-3, direct strut AC, which directly transfers some of the load acting on the support to the loading point, is additionally applied. In this case, because the model becomes statically indeterminate, the compressive force of the direct strut (C_d) is calculated in the CEB-FIP model code (1993) and Foster model (Foster, 1998; Foster & Gilbert, 1998) using Eqs. (1) and (2), respectively. Design is then performed using the

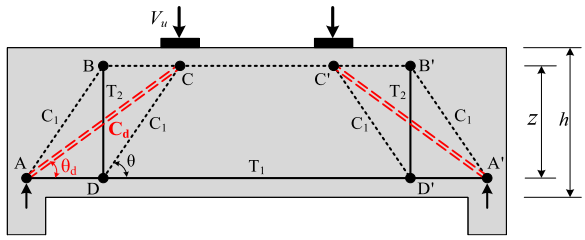

Fig. 10 STM with direct struts (STM-3)

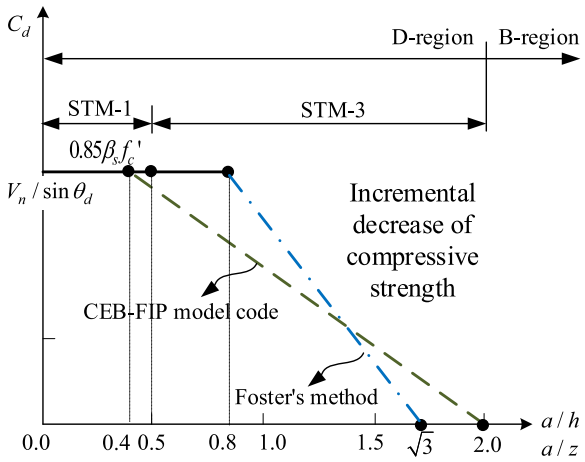

Fig. 11 Force acting on the direct strut

statically determinate STM for the reduced shear load ($V_u - C_d sin\theta_d$).

CEB-FIP model code (1993)

$$C_d = \left(\frac{4 - 2a/z - N/V_n}{3 - N/V_n}\right)\frac{1}{sin\theta_d}V_n, T_2 = V_n - C_d sin\theta_d \quad (1)$$

Foster model (Foster, 1998; Foster & Gilbert, 1998)

$$C_d = \left(\frac{\sqrt{3} - a/z}{\sqrt{3} - 1}\right)\frac{1}{sin\theta_d}V_n, T_2 = V_n - C_d sin\theta_d \quad (2)$$

where, T_2: the tensile force of the intermediate vertical tie, z: the distance between the centers of the upper and lower chords,θ_d: the angle of the direct strut, and N: the axial force.

C_d in Eqs. (1) and (2) is calculated according to the geometric condition of the member. If the a/z decreases, as shown in Fig. 11, the load transferred by the direct strut increases, but the member force resisted by the vertical shear reinforcement (T_2) decreases. In contrast, if the a/z increases, the load transferred by the direct strut decreases, and the member force of T_2 increases. In Eq. (1), the total shear force (V_n) is transferred only by the direct strut at$a/z \leq 0.5$. Therefore, $T_2 = 0$ and the model is changed from STM-3 to STM-1. At$a/z = 2$, the total shear force must be supported by intermediate vertical ties, because no shear force is transferred by direct struts ($T_2 = V_n$). The Foster model of Eq. (2) is also changed from STM-3 to STM-1 at$a/z \leq 1.0$. In addition, because T_2 depends on a/z in Eqs. (1) and (2), the amount of vertical reinforcement to be placed gradually decreases, causing no discontinuity in the amount of reinforcement or strength at the boundary between STM-1 and STM-3. Therefore, in this study, the maximum strength limit evaluation equation for deep beams was developed using STM-3 with direct struts.

3.3 Discontinuity in the Effective Compressive Strength of Concrete

In the CEB-FIP model code (1993) and Foster model (Foster, 1998; Foster & Gilbert, 1998), the portion of the load acting on the direct strut, which varies depending on a/z, is calculated using Eq. (1) or (2). It is the portion of the external force acting on the direct strut, rather than the resistance force. Therefore, the resistance force (strength) of the direct strut, which depends on a/z, must be calculated to determine the $V_{n,max}$ of the deep beam using STM-3.

The effective concrete compressive strength of the interior strut $\left(\xi f_c'\right)$ is closely related to a/h. The $\xi f_c'$ of a member whose a/h is 0 is identical to that of the boundary strut ($\xi f_c' = 0.85\ f_c'$ in the ACI 318–19 code (2019)) because it is subjected to uniaxial compressive force. If a/h increases, $\xi f_c'$ decreases because the interior strut is subjected to biaxial stresses ($\xi f_c' = 0.85\ \beta_s f_c'\ \xi f_c'$ in the ACI 318–19 code (2019)). The $\xi f_c'$ differs among different codes. Fig. 12 shows the $\xi f_c'$ of RC beams with f_c' =40 MPa. Here, the characteristics of $\xi f'_c$ can be observed as follows.

1) In the ACI 318–19 code (2019), for deep beams with $a/h \leq 2.0$, the constant $\xi f_c'$ is used regardless of a/h. The effective compressive strength coefficient of concrete (ξ) is 0.75 or 0.4, depending on the member type. EC2-04 (2004) also uses the constant $\xi = 0.6\left(1 - f_c'/250\right)$.

2) In the AS 3600 code (2009), ξ is calculated using Eq. (3) according to the research results of Foster and Malik (2002). In Eq. (3), since the angle of the strut (θ) decreases as a/h increases, $\xi f_c'$ decreases as a/h increases, as shown in Fig. 12.

$$\xi = 0.9 \times \frac{1}{1 + 0.66(cot\theta)^2}, 0.27 \leq \xi \leq 0.9 \quad (3)$$

3) Since $\xi = 0.6\left(1 - f_c'/250\right)$ is also used for the beams with $\frac{a}{h} > 2.0$ in the EC2-04 (2004), there is no discontinuity in the ξ at $a/h = 2.0$. However, the shear

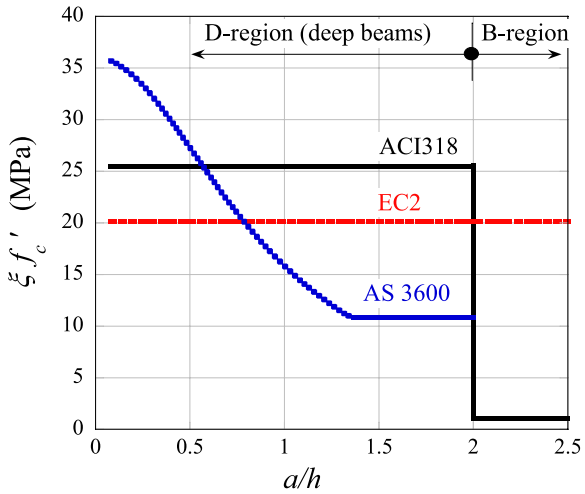

Fig. 12 Comparison of the effective compressive strength of the concrete strut among three codes

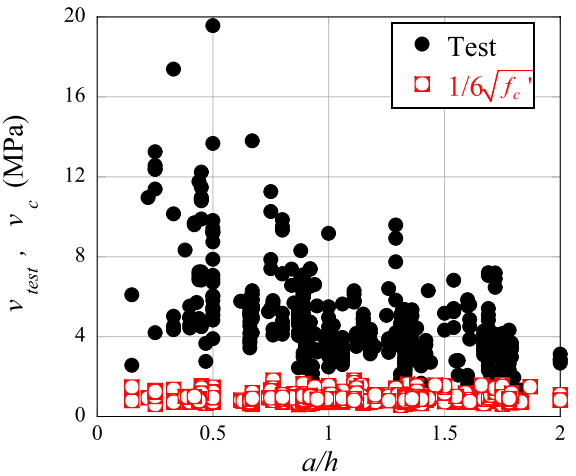

Fig. 13 v_{test} vs. $v_c = (1/6) \times \sqrt{f_c'}$ for the 672 deep beams

strength contribution of concrete in the B-region (v_c, Table 22.5.5.1) is used for the beams with $a/h > 2.0$ in the ACI 318–19 code (2019). Therefore, a discontinuity occurs at $a/h = 2.0$ in the ACI 318–19 code (2019).

To examine that the $\xi f_c'$ of deep beams is constant at $a/h \leq 2.0$, as shown in Fig. 12, the experimental data for the 672 specimens were analyzed. Fig. 13 presents the relationship between the shear strength ($v_{test} = V_{test}/(bd)$) and a/h for the 672 deep beams. In Fig. 13, the concrete shear resistance of the ACI 318–19 codes ($v_c = (1/6) \times \sqrt{f_c'}$) and the v_{test} of the specimens were compared. Fig. 13 clearly shows that v_{test} decreased as a/h increased. Therefore, it is reasonable that $\xi f_c'$ also decreases as a/h increases, as with the ξf_c of the AS 3600 code (2009). This result was obtained in several previous studies on deep beams (Brown, 2005; Larson et al., 2013; Smith & Vantsiotis, 1982), as well as the present analysis. In the comparison between the v_c in the ACI 318–19 code (2019) and the v_{test} of the specimens, $v_c = (1/6) \times \sqrt{f_c'}$ is the lower limit of the shear strength of the 672 specimens, which differs significantly from the v_{test} of the specimens with small a/h. However, there is no significant difference from the experimental values at $a/h = 2$. This indicates that the shear strength of members with $a/h = 2$ can be designed with $v_c = (1/6) \times \sqrt{f_c'}$ via the B-region method.

3.4 Maximum Shear Strength Considering the Effective Compressive Strength of Concrete

The maximum shear strength of general beams ($a/h \geq 2.0$) or walls is based on the concept of under-reinforced failure, in which concrete fails after the yielding of steel reinforcement. Therefore, the strength of concrete must be directly compared with that of steel reinforcement to determine the maximum shear strength (EC2-04, 2004; Lee et al., 2021; Lee & Hwang, 2010). However, in the design of deep beams, it is difficult to determine the maximum shear strength limit by directly comparing the strengths of the two materials. As mentioned in Fig. 9, this is because the minimum reinforcement is placed when STM-1 is used. In this case, since $V_{n,max}$ is determined by the strength of the tie, $V_{n,max}$ is inevitably lower than the actual limit (Lee & Kang, 2021). In contrast, when STM-2 is used, since the member force of vertical tie BD is identical to the factored load V_u as shown in Fig. 8, the amount of steel reinforcement resisting V_u must be placed. Thus, $V_{n,max}$ is inevitably greater than the actual limit (Lee & Kang, 2021).

As explained previously, $V_{n,max}$ must reflect the change in the strength of members. When STM-1 or STM-2 of ACI Subcommittee 445 (ACI Committee 445, 2002) is used, a discontinuity occurs in the required steel reinforcement. In addition, as shown in Fig. 12, for the ACI 318–19 (2019) and AS 3600 codes (2009), $\xi f_c'$ involves a discontinuity at $a/h = 2$. For the ACI 318–19 code (2019) and EC2-04 (2004), $\xi f_c'$ is unaffected by a/h. Herein, a maximum strength evaluation equation for deep beams was developed using the $\xi f_c'$ of the concrete strut without discontinuity. The proposed $\xi f_c'$ is identical to the $\xi f_c'$ of the ACI 318–19 code (2019) at $a/h \leq 0.5$, as shown in Fig. 14. However, as a/h increases, it decreases linearly and becomes identical to $v_{c,max} = (5/6) \times \sqrt{f_c'}$, which is the $V_{n,max}$ of the B-region beam, at $a/h = 2.0$.

1) As indicated by the comparison of the 672 specimens in Fig. 13, the shear strength of a member with $a/h = 2$ can be calculated using the B-region design method. Therefore, the maximum shear strength

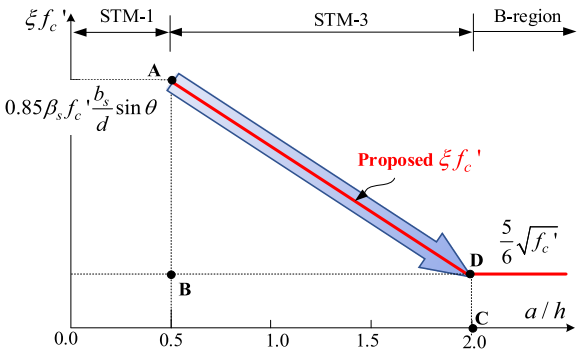

Fig. 14 Effective compressive strength of the concrete strut

limit ($(5/6) \times \sqrt{f_c'}$) for general beams can also be used as the strength limit of the beams with $a/h = 2$.

2) Fig. 14 is based on the same concept as STM-3 in Fig. 10. The total shear force (V_n) is transferred only by the direct strut at $a/h \leq 0.5$, and the model is changed from STM-3 to STM-1. Additionally, it is changed to B-region shear design at $a/h = 2.0$. Therefore, the discontinuity of $\xi f_c'$ according to a/h does not occur. In this study, the boundary point between STM-1 and STM-3 was set as $a/h = 0.5$. This is because 2.5 times the shear strength of general beams is maintained when a/h is ≤ 0.4 in the equation of De Paiva and Siess[2], which was used in the ACI 318 code until 2003. In the CEB-FIP model code (1993), the boundary point between STM-1 and STM-3 is set as $a/z = 0.5$. In this study, the boundary point between the models was set as $a/h = 0.5$, in accordance with the CEB-FIP model code (1993) and the equation of De Paiva and Siess (1965).

$\xi f_c'$ at $0.5 \leq a/h \leq 2.0$ can be calculated as follows:

$$f_{ce} = \xi f_c' = \mathrm{B} - \frac{B-A}{1.5}\left(2 - \frac{a}{h}\right) \tag{4}$$

where $A = \xi f_c' \sin(\theta) = 0.85 \times \beta_s \times f_c' \frac{b_s}{d} \sin(\theta)$ is the vertical component of $\xi f_c'$ at $a/h = 0.5$. $B = 5/6\sqrt{f_c'}$ is equal to $v_{n,max}$ at $a/h = 2.0$. For calculating A, b_s/d was multiplied by the effective area of the concrete strut to convert it into the total area. According to the lower bound plastic theory of Nielsen (Nielsen et al., 1978) and Watanabe and Ichinose (1991), the strength must be the highest value among the values obtained from the statically allowed stress field. Thus, the effective height of the strut (b_s) can be set as $0.5z$. (Watanabe & Ichinose, 1991) β_s is the strut coefficient, and the values in Table 23.4.3(a) of ACI 318–19 (2019) or simply 0.75 can be used. Because $A = \xi f_c'$ at $a/h = 0.5$, θ is 58° when the distance between the centers of the upper and lower chords is $0.8h$. In addition, $A = 0.34\beta_s f_c' \sin(58^\circ)$ because $0.5z \simeq 0.4d$. Finally, the maximum strength of deep beams is calculated as follows:

$$V_{n,max} = f_{ce} b_w d = \left[\mathrm{B} - \frac{B-A}{1.5}\left(2 - \frac{a}{h}\right)\right] b_w d \tag{5}$$

where $A = 0.288\beta_s f_c'$ and $B = 5/6\sqrt{f_c'}$. As a result, $A = 0.216 f_c'$, which is similar to that of the AASHTO-LRFD code ($0.225 f_c'$).

4 Verification of Proposed Maximum Shear Strength Model

Fig. 15 presents a comparison of the $V_{n,max}$ of the different codes with the value calculated using Eq. (5). As shown in Fig. 15a, the $V_{n,max}$ of Eq. (5) was lower than that of the AASHTO-LRFD code (2020) but higher than that of the ACI 318–19 code (2019). The $V_{n,max}$ of Eq. (5) increased in proportion to f_c' similar to the $V_{n,max}$ of the AASHTO-LRFD code (2020). Therefore, the $V_{n,max}$ of the three equations were similar for members normal-strength concrete, but the $V_{n,max}$ of Eq. (5) and the AASHTO-LRFD code (2020) were higher than that of the ACI 318–19 code (2019) for members having high-strength concrete.

Fig. 15b compares the $V_{n,max}$ of members with f_c' = 40 MPa. At $a/h \leq 0.5$, $v_{n,max} = 0.216 f_c' = 8.64$ MPa from Eq. (5) was almost identical to $v_{n,max} = 0.225 f_c' = 9.0$ MPa from the AASHTO-LRFD code (2020). However, $v_{n,max} = 5/6\sqrt{f_c'} = 5.27$ MPa from the ACI 318–19 code (2019) was much smaller than those of Eq. (5) and the AASHTO-LRFD code (2020). At $a/h = 2.0$, the $v_{n,max}$ of Eq. (5) and the ACI 318–19 code (2019) were identical ($5/6\sqrt{f_c'} = 5.27$ MPa), and that of the AASHTO-LRFD code (2020) was far greater ($0.225 f_c' = 9.0$ MPa). For the AASHTO-LRFD (2020) and ACI 318–19 codes (2019), $V_{n,max}$ was constant with an increase in a/h, but that of Eq. (5) decreased when a/h increased, similar to the $\xi f_c'$ of the AS 3600 code (2009). In addition, no discontinuity occurred at $a/h = 2.0$, because the $V_{n,max}$ of Eq. (5) was identical to that of the B-region ($5/6\sqrt{f_c'}$).

4.1 Influence of Compressive Strength of Concrete

Proestose et al. (2018) performed an experiment on large-size RC members to identify the maximum shear strength limit. According to their results, the current ACI 318–19 code (2019) limit significantly underestimated the $v_{n,max}$ of deep beams, while the AASHTO-LRFD (2020) limit provided an accurate estimate of the maximum shear capacity. In the present study, the maximum strength was compared, as shown in Fig. 16a and Table 2, for the four specimens tested by Proestose et al.

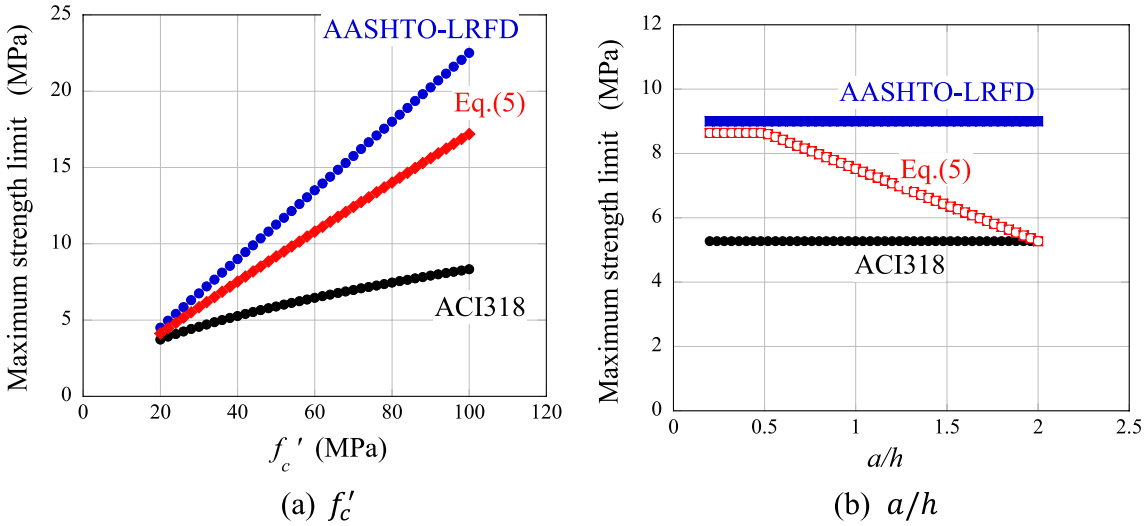

Fig. 15 Comparison of $V_{n,max}$ among different design codes

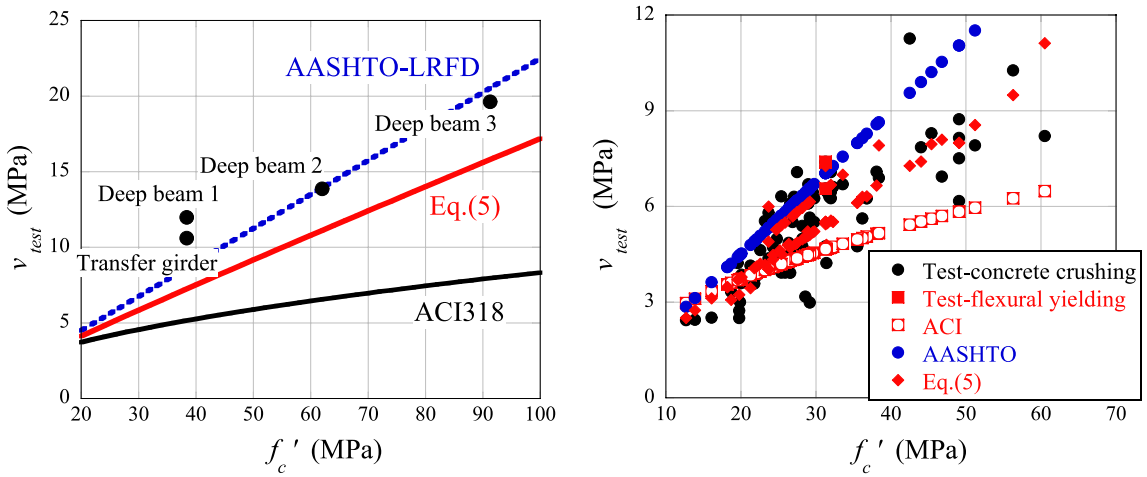

Fig. 16 Comparison of shear-strength limits according to the compressive strength of concrete

Table 2 Strength ratio of transfer girder and three deep beams

Specimen	V_{test} (kN)	v_{test} (MPa)	v_{test}/v_{ACI} (MPa)	v_{test}/v_{AASHTO} (MPa)	$v_{test}/v_{Eq.(5)}$ (MPa)
Transfer girder	1767	10.6	2.06	1.23	1.46
Deep beam 1	1469	12.0	2.33	1.39	1.65
Deep beam 2	1700	13.9	2.12	0.99	1.25
Deep beam 3	1393	19.6	2.85	0.96	1.25
	Mean		2.34	1.14	1.40

(2018). As indicated by the figure, the $v_{n,max}$ of the ACI 318–19 code (2019) was low, as in the results of Proestose et al. (2018). In particular, for members that used high-strength concrete, $v_{n,max}$ was only 39% of the actual value, which making the design uneconomical. In contrast, the $v_{n,max}$ of the AASHTO-LRFD code (2020) accurately predicted the maximum strengths of members. Equation (5) provided $v_{n,max}$ lower than the AASHTO-LRFD (2020) limit but similarly predicted changes in the shear strength of members, which increased according to f_c'.

Fig. 16b presents a comparison of the shear strengths of the 85 specimens used in the analysis of Figs. 3 and 4 with the $v_{n,max}$ calculated using the three methods. As shown in the figure, the $v_{n,max}$ of the ACI 318–19 code (2019) was excessively low regardless of the failure mode, as in the comparison results for the four specimens tested by Proestose et al. (2018). In comparison, the AASHTO-LRFD code (2020) and Eq. (5) reflected the influence of f_c' on $v_{n,max}$ more accurately.

4.2 Influence of Shear Span-to-Depth Ratio

The influence of the shear span-to-depth ratio (a/h) is not reflected for the $v_{n,max}$ of the ACI 318–19 (2019) and AASHTO-LRFD codes (2020). However, in many experiments, the shear strength of deep beams decreased as a/h increased. Fig. 17a presents a comparison of the experimental results of Proestose et al. (2018) with $v_{n,max}$. For the specimens used, shear failure occurred before the yielding of the longitudinal tensile reinforcement. As shown in the figure, the shear strength decreased as a/h increased. For the ACI 318–19 (2019) and AASHTO-LRFD codes (2020), $v_{n,max}$ was constant despite the increase in a/h, similar to the results of Fig. 6. Therefore, for the specimens with large a/h, the $v_{n,max}$ of the AASHTO-LRFD code (2020) overestimates the maximum strength limit.

Fig. 17b presents a comparison of the shear strengths of the 34 specimens used in the analysis of Figs. 5 and 6. The 34 specimens had different a/h even though f_c' was approximately 45 MPa. For the 34 specimens, the shear strength decreased as a/h increased. Additionally, the $v_{n,max}$ of Eq. (5) decreased as a/h increased, accurately reflecting the influence of a/h.

4.3 Influence of Size Effect

The experimental data for the 672 specimens included results for various variables, and it was difficult to directly evaluate the size effect. Therefore, in this study, the experimental results of Walraven and Lehwalter (1994) and Watanabe et al.(2008), in which the influence of the size effect was directly measured, were used among the collected data. As the f_c' of 25 specimens ranged from 18.2 to 36.8 MPa, the strengths (v_{test}) of the specimens were divided by f_c' for nondimensionalization.

Equation (5) proposed herein did not consider the size effect. Therefore, $v_{n,max}$ was calculated by multiplying Eq. (5) by the size-effect modification factor λ_s, which was used in the ACI318-19 code (ACI318-19 22.5.5.1.3). In Fig. 18, $v_{n,max}$ was calculated by multiplying Eq. (5) by the λ_s. From the Fig. 18, it can be seen that the $v_{n,max}$ considering the size effect predicts the actual strength limit with reasonable agreement. Similarly, it is judged that the influence of the size effect can be considered, if the $v_{n,max}$ is multiplied by the λ_s of the design code.

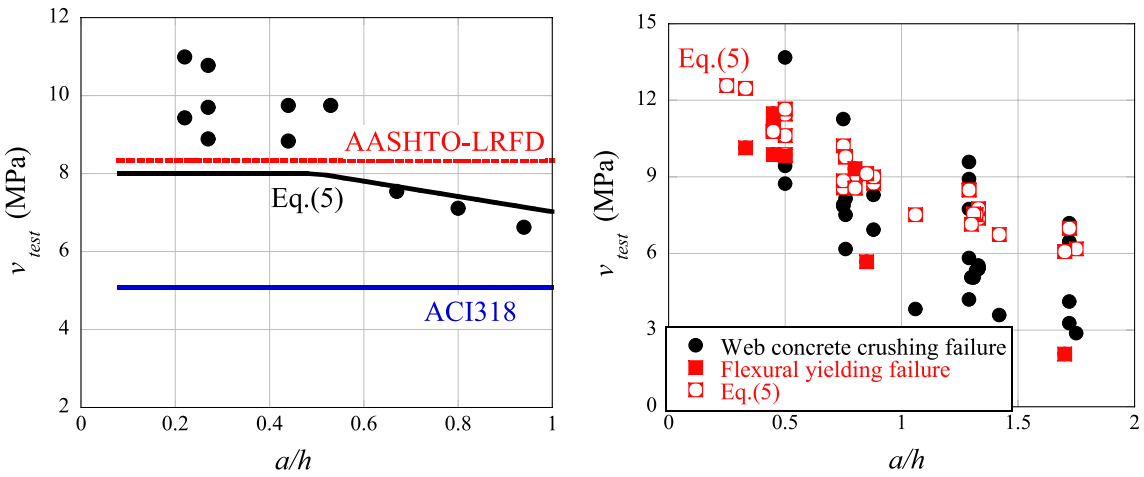

(a) Experimental results of Proestos et al (b) 34 specimens

Fig. 17 Comparison of shear-strength limits according to the shear span-to-depth ratio

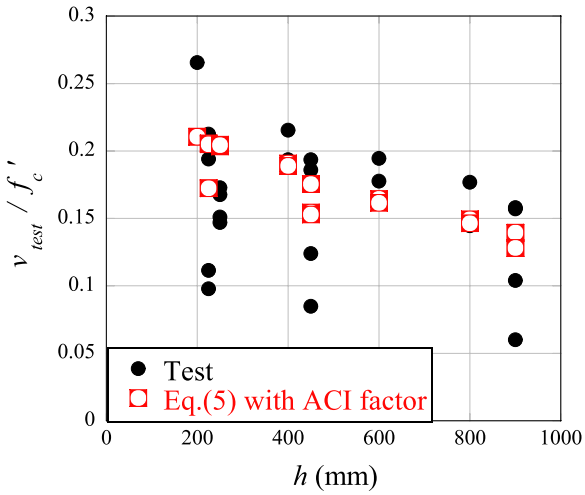

Fig. 18 Relationship between the section depth and v_{test}/f_c'

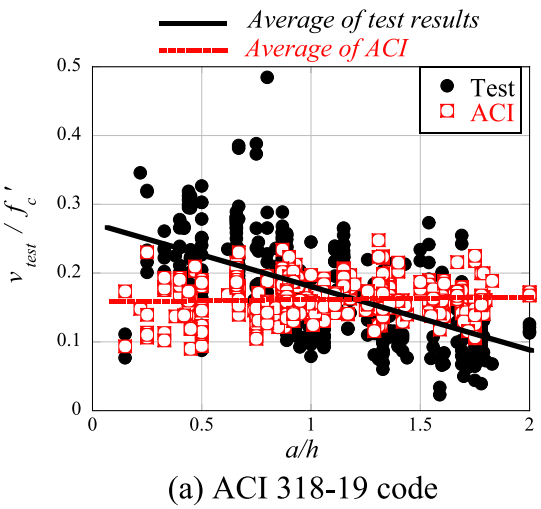

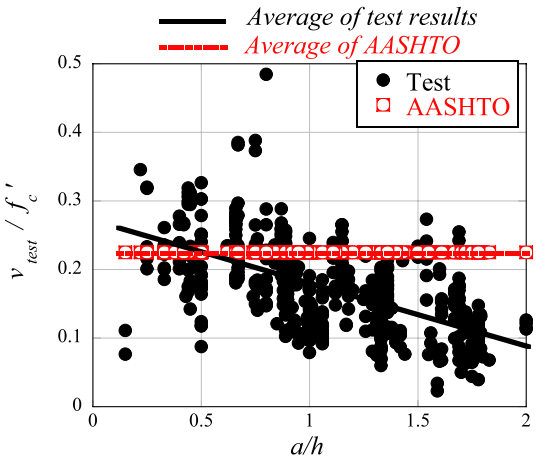

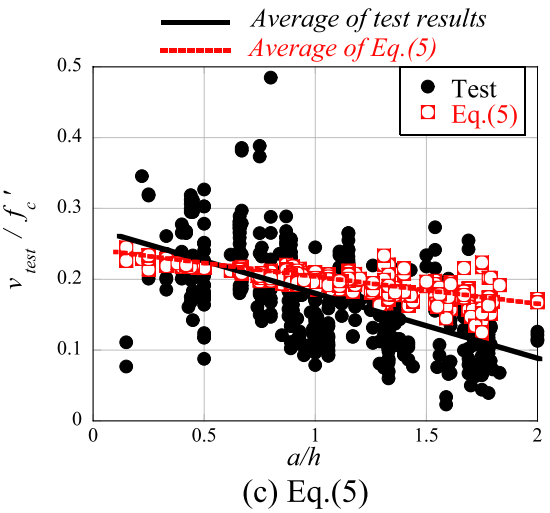

Fig. 19 Comparison of the $v_{n,max}$ values of the three codes with the strengths of the 672 specimens

4.4 Comparison of Experimental Data for 672 Specimens

The shear strengths of the 672 deep beam specimens were compared with the $v_{n,max}$ of the ACI 318–19 code (2019), the AASHTO-LRFD code (2020), and proposed Eq. (5). Fig. 19 presents a comparison of the calculated $v_{n,max}$ with the experimental results. The effects of f_c' and a/h on $v_{n,max}$ were examined. As shown in Fig. 18, if the size effect is reflected in Eq. (5), the prediction accuracy of the proposed equation is improved. However, the λ_s of ACI 318–19 code can be applied to general beams and only to specimens with steel reinforcement below the minimum reinforcement ratio. Therefore, in this study, $v_{n,max}$ was calculated without considering the size effect.

Theoretically, $v_{n,max}$ must be higher than v_n because it is the maximum strength value. However, in Fig. 19, the $v_{n,max}$ of the ACI 318–19 code [6] is approximately the average value of the actual strength (v_{test}). In particular, at $a/h \leq 0.5$, $v_{n,max}$ was far lower than the average of v_{test}. The $v_{n,max}$ values of the AASHTO-LRFD code [9] and Eq. (5) were similar at $a/h \leq 0.5$. The $v_{n,max}$ of the AASHTO-LRFD code [9] remained constant regardless of a/h, exhibiting a difference from the average of v_{test} at $a/h = 2$. The $v_{n,max}$ of Eq. (5) predicted v_{test} with reasonable agreement. The strengths of the specimens and the $v_{n,max}$ of Eq. (5) decreased as a/h increased.

Quantitative evaluation can show the accuracy of the proposed equation more clearly (Leelatanon et al., 2022; Setkit et al., 2021). Equation (5) and the two design codes were quantitatively compared. The value of $v_{n,max}$ must account for factors affecting the shear strength of deep beam. Therefore, the shear strength ratio ($v_{test}/v_{n,max}$) of 672 specimens was compared, as shown in Fig. 20. The coefficient of variation (COV) of $v_{test}/v_{n,max}$ for the ACI318-19 code was 39.2%, while that

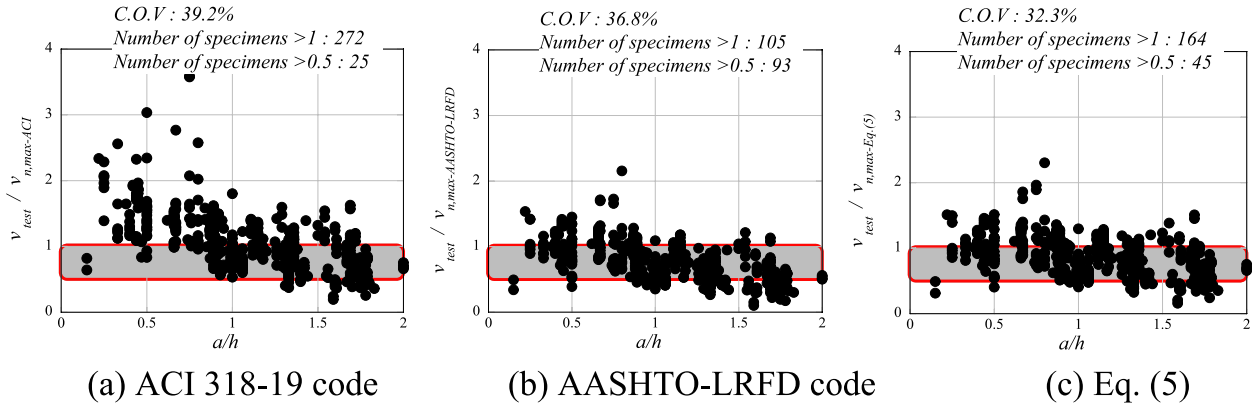

Fig. 20 Comparison of the $v_{test}/v_{n,max}$ values. **a** ACI 318–19 code, **b** AASHTO-LRFD code, **c** Eq. (5)

of Eq. (5) was 32.3%, which was the smallest among the three predictions. Unlike general predictions of shear strength, predictions for $v_{n,max}$ must consider both safety and economy. Since $v_{n,max}$ represents the maximum strength value, the value of $v_{test}/v_{n,max}$ should ideally be less than 1. However, if $v_{test}/v_{n,max}$ is too small, it can indicate a potential unsafe prediction because $v_{n,max}$ would not appropriately limit v_{test} based on material properties. Therefore, the number of specimens with $v_{test}/v_{n,max} > 1.0$ or $v_{test}/v_{n,max} < 0.5$ was compared, as shown in Fig. 20. The ACI318-19 code predicted uneconomical for 272 (40.5%) out of 672 specimens with $v_{test}/v_{n,max} > 1.0$, while the AASHTO-LRFD code predicted riskily for 93 specimens (13.8%) with $v_{test}/v_{n,max} < 0.5$. The prediction results of Eq. (5) were intermediate between the ACI and AASHTO predictions, providing a reasonable balance between economy and safety.

5 Conclusions

Strength limits specified in the RC design codes are necessary for safe design. However, if such limits are excessively low, the design may be uneconomical, and if they are too high, the design may be dangerous. The maximum shear strength limit of deep beams in the ACI 318–19 code is identical to that of general beams and tends to underestimate the actual strength of deep beams. Herein, an equation for calculating the maximum shear strength of deep beams was proposed with consideration of the compressive strength of concrete and shear span-to-depth ratio. The maximum strength limits of the currently used codes and proposed equation were compared with experimental data for 672 deep beam specimens to evaluate their suitability. The results of this study are summarized as follows;

1) The $v_{n,max}$ of the ACI 318–19 code significantly underestimated the strength of deep beams with high-strength concrete. However, the $v_{n,max}$ of the AASHTO-LRFD code closely matched the experimental data. Among the 85 specimens analyzed, the maximum shear strength, $v_{n,max}$ predicted by the ACI 318–19 code was lower than the experimental shear strength, v_{test} in 65 cases (76.5%), whereas the AASHTO-LRFD code underestimated v_{test} in only 12 cases (14.1%).
2) The ACI 318–19 code conservatively limited the strength of deep beams with small a/h values, while the AASHTO-LRFD code excessively limited the strength of deep beams with large a/h values.
3) The influence of f_c' and a/h were reflected in the proposed maximum strength limit equation for deep beams. The proposed equation predicted $v_{n,max}$ more accurately than both the ACI 318–19 and AASHTO-LRFD codes. The coefficient of variation of $v_{test}/v_{n,max}$ was 39.2% for the ACI318-19 code, while it was reduced to 32.3% using the proposed equation.

The analytical results indicated incorporating the size effect into Eq. (5) improved the prediction accuracy of the proposed equation. However, the $v_{n,max}$ of Eq. (5) was calculated without considering the size effect, as its influence was not directly examined in this study. Therefore, further studies are needed to develop $v_{n,max}$ while accounting for the size effect.

Abbreviations

a	Shear span
b_s	Effective height of concrete strut
b_w	Width of beam cross-section
C_d	Compressive force of direct strut
d	Effective depth of beam cross-section
f_c'	Compressive strength of concrete
f_{ce}	Effective compressive strength of concrete strut
f_{yv}	Yield strength of vertical shear reinforcement
h	Depth of beam cross-section

N	The axial force ("+" for tensile force)
T_2	Tensile force of vertical tie
v_c	Shear stress of concrete
V_c	Shear strength provided by concrete
V_{test}	Measured shear strength by experiment
V_n	Nominal shear strength
$V_{n,max}$	Maximum shear strength
V_s	Shear strength provided by stirrup
V_u	Factored shear force
z	Distance between the upper and lower chords
ρ_h	Horizontal shear reinforcement ratio
ρ_v	Vertical shear reinforcement ratio
$\rho_{v,min}$	Minimum ratio of vertical shear reinforcement
β_s	Effective compressive strength factors of concrete in strut
θ	Angle between axis of strut and the tension chord of the members
θ_d	Angle between direct strut and lower tie
ξ	*effective* Compressive strength coefficient of concrete

Supplementary Information

The online version contains supplementary material available at https://doi.org/10.1186/s40069-025-00814-z.

Additional file 1.

Acknowledgements
Not applicable.

Author contributions
Jung-Yoon Lee: conceptualization, investigation, analysis and validation, writing–original draft, review & editing. Yeonje Choi: experimental assistance, data curation, analysis. Donglk Shin: conceptualization, experimentation, validation, Data acquisition, formal analysis, writing–review & editing.

Funding
This research was supported by the Basic Science Research Program through the National Research Foundation of Korea (NRF), funded by the Ministry of Education (RS-2022-NR070436).

Data availability
The authors declare that the datasets used or analyzed during the current study are available from the corresponding author on reasonable request.

Declarations

Ethics approval and consent to participate
Not applicable.

Consent for publication
Not applicable.

Competing interests
The authors declare that they have no competing interests.

Received: 17 November 2024 Accepted: 13 June 2025
Published online: 09 September 2025

References

AASHTO LRFD. (2020). Bridge Design Specifications, 9th Edition. Washington, DC, American Association of State Highway Transportation Officials.
ACI Committee 318 .(1999). 318–99/318R-99: Building Code Requirements for Structural Concrete & Commentary. American Concrete Institute.
ACI Committee 318. (2002). Building code requirements for structural concrete:(ACI 318–02) and commentary (ACI 318R-02). American Concrete Institute.
ACI Committee 318. (2019). *Building Code Requirements for Structural Concrete (ACI 318–19) and Commentary (ACI 318R–19)*. American Concrete Institute.
ACI Committee 445. (2002). *Examples for the design of structural concrete with strut-and-tie models*. American Concrete Institute.
BD-002 Concrete Structures Committee. (2009). *AS 3600–2009—Standards for concrete structures*. Standards.
Bediwy, A. G., & El-Salakawy, E. F. (2021). Ductility and performance assessment of glass fiber-reinforced polymer-reinforced concrete deep beams incorporating cementitious composites reinforced with basalt fiber pellets. *ACI Structural Journal, 118*(4), 83–95. https://doi.org/10.14359/51732646
Brown, M. D. (2005). *Design for shear in reinforced concrete using strut-and-tie and sectional models*. The University of Texas at Austin.
Comité Euro-International du Béton. (1993). *0727739441: CEB-FIP model code 1990: Design code*. Thomas Telford Publishing.
Comité Européen de Normalisation (CEN). (2004). *Eurocode 2: Design of concrete structures, Part 1–1 general rules and rules for buildings (EC2-04)*. CEN.
Crist, R. A. (1966). Shear behavior of deep reinforced concrete beams. In Symposium on the Effects of RepeatedLoading of Materials and Structural Elements (Mexico City, 1966), vol. 4, pp. 31.
CSA Committee A23.3–19. (2019). *Design of concrete structures for buildings (CSA A23.3–19)*. Canadian Standards Association.
de Paiva, H. R., & Siess, C. P. (1965). Strength and behavior of deep beams in shear. *Journal of the Structural Division, 91*(5), 19–41. https://doi.org/10.1061/JSDEAG.0001329
Foster, S. J. (1998). Design of non-flexural members for shear. *Cement and Concrete Composites, 20*(6), 465–475. https://doi.org/10.1016/S0958-9465(98)00029-8
Foster, S. J., & Gilbert, R. I. (1998). Experimental studies on high-strength concrete deep beams. *ACI Structural Journal, 95*(4), 382–390. https://doi.org/10.14359/554
Foster, S. J., & Malik, A. R. (2002). Evaluation of efficiency factor models used in strut-and-tie modeling of nonflexural members. *Journal of Structural Engineering, 128*(5), 569–577. https://doi.org/10.1061/(ASCE)0733-9445(2002)128:5(569)
Hwang, S. J., Yang, Y. H., & Li, Y. A. (2021). Maximum shear strength of reinforced concrete deep beams. *ACI Structural Journal, 118*(6), 155–164. https://doi.org/10.14359/51733076
Imjai, T., Aosai, P., Garcia, R., Raman, S. N., & Chaudhary, S. (2024). Deflections of high-content recycled aggregate concrete beams reinforced with GFRP bars and steel fibres. *Engineering Structures, 312*, 118247. https://doi.org/10.1016/j.engstruct.2024.118247
Imjai, T., Guadagnini, M., Garcia, R., & Pilakoutas, K. (2016). A practical method for determining shear crack induced deformation in FRP RC beams. *Engineering Structures, 126*, 353–364. https://doi.org/10.1016/j.engstruct.2016.08.007
Imjai, T., Kefyalew, F., Aosai, P., Garcia, R., Kim, B., Abdalla, H. M., & Raman, S. N. (2023). A new equation to predict the shear strength of recycled aggregate concrete Z push-off specimens. *Cement and Concrete Research, 169*, 107181. https://doi.org/10.1016/j.cemconres.2023.107181
Kong, F. K. (1990). *Reinforced concrete deep beams*. Van Nostrand Reinhold.
Larson, N., Gomez, E. F., Garber, D., Bayrak, O., & Ghannoum, W. (2013). *Strength and serviceability design of reinforced concrete inverted-T beams*. Report.
Lee, J. Y., Haroon, M., Shin, D., & Kim, S. W. (2021). Shear and torsional design of reinforced concrete members with high-strength reinforcement. *Journal of Structural Engineering, ASCE, 147*(2), 04020327. https://doi.org/10.1061/(ASCE)ST.1943-541X.0002887
Lee, J. Y., & Hwang, H. B. (2010). Maximum shear reinforcement of reinforced concrete beams. *ACI Structural Journal, 107*(5), 580–588. https://doi.org/10.14359/51663909
Lee, J. Y., & Kang, Y. M. (2021). Strut-and-tie model without discontinuity for reinforced concrete deep beams. *ACI Structural Journal, 118*(5), 123–134. https://doi.org/10.14359/51732824
Leelatanon, S., Imjai, T., Setkit, M., Garcia, R., & Kim, B. (2022). Punching shear capacity of recycled aggregate concrete slabs. *Buildings, 12*(10), 1584. https://doi.org/10.3390/buildings12101584
Ms, S., Nagarajan, P., & AP, S. (2022). Behavior of steel fiber-reinforced rubcrete deep beams under shear. *ACI Structural Journal, 119*(1), 15–25. https://doi.org/10.14359/51733003
Nielsen, M., Braestrup, M., Jensen, B. & Bach, F. (1978). Concrete Plasticity: Beam Shear—Shear in Joints—Punching Shear. *Danish Society for Structural Science and Engineering*, 1–129.

Proestos, G. T., Bentz, E. C., & Collins, M. P. (2018). Maximum shear capacity of reinforced concrete members. *ACI Structural Journal, 115*(5), 1463–1473. https://doi.org/10.14359/51702252

Rogowsky, D. M., MacGregor, J. G., & Ong, S. Y. (1986). Tests of reinforced concrete deep beams. *ACI Journal Proceedings., 83*, 614–623.

Russo, G., Somma, G., & Mitri, D. (2005). Shear strength analysis and prediction for reinforced concrete beams without stirrups. *Journal of Structural Engineering, 131*(1), 66–74. https://doi.org/10.1061/(ASCE)0733-9445(2005)131:1(66)

Setkit, M., Leelatanon, S., Imjai, T., Garcia, R., & Limkatanyu, S. (2021). Prediction of shear strength of reinforced recycled aggregate concrete beams without stirrups. *Buildings, 11*(9), 402. https://doi.org/10.3390/buildings11090402

Shin, S. W., Lee, K. S., Moon, J. I., & Ghosh, S. K. (1999). Shear strength of reinforced high-strength concrete beams with shear span-to-depth ratios between 1.5 and 2.5. *ACI Structural Journal, 96*(4), 549–556. https://doi.org/10.14359/691

Smith K. & Vantsiotis A. (1982). Shear strength of deep beams. In *ACI Journal Proceedings*, pp. 201–213.

Tan, K., & Cheng, G. (2006). Size effect on shear strength of deep beams: Investigating with strut-and-tie model. *Journal of Structural Engineering, 132*(5), 673–685.

Walravena, J., & Lehwalter, N. (1994). Size effects in short beams loaded in shear. *ACI Structural Journal, 91*(5), 585–593. https://doi.org/10.14359/4177

Watanabe F & Ichinose T. (1991). Strength and ductility design of RC members subjected to combined bending and shear. In *Proceedings of Workshop on Concrete in Earthquake*. University of Houston Texas, USA, pp. 429–438.

Watanabe, M., Tanaka, Y., & Shimomura, T. (2008). Size-effect of shear strength and estimation method of shear capacity of deep beam. *Journal of JSCE, 64*(4), 683–697. https://doi.org/10.2208/jsceje.64.683

Yang, K. H., Chung, H. S., Lee, E. T., & Eun, H. C. (2003). Shear characteristics of high-strength concrete deep beams without shear reinforcements. *Engineering Structures, 25*(10), 1343–1352. https://doi.org/10.1016/S0141-0296(03)00110-X

Zhang, N., & Tan, K. H. (2007). Size effect in RC deep beams: Experimental investigation and STM verification. *Engineering Structures, 29*(12), 3241–3254. https://doi.org/10.1016/j.engstruct.2007.10.005

Publisher's Note

Jung-Yoon Lee Professor, School of Civil, Architectural Engineering and Landscape Architecture at Sungkyunkwan University, 2066, Seobu-Ro, Jangan-Gu, Suwon-Si, Gyeonggi-Do, 16,419, Republic of Korea.

Yeonje Choi Graduate student, Department of Civil, Architectural, and Environmental System Engineering at Sungkyunkwan University, 2066, Seobu-Ro, Jangan-Gu, Suwon-Si, Gyeonggi-Do, 16,419, Republic of Korea.

Donglk Shin Post—Doctoral Researcher of Global Engineering Institute for Ultimate Society at Sungkyunkwan University, 2066, Seobu-Ro, Jangan-Gu, Suwon-Si, Gyeongg i-Do, 16,419, Republic of Korea.